Research Article

Suicide transport blockade of motor neuron survival generates a focal graded injury and functional deficit

https://doi.org/10.4103/1673-5374.301032

Date of submission: April 29, 2020

Date of decision: June 10, 2020

Date of acceptance: August 13, 2020

Date of web publication: December 12, 2020

Allison S. Liang[1], Joanna E. Pagano[1], Christopher A. Chrzan[1], Randall D. McKinnon[1, 2, *]

Graphical Abstract *Backdoor intrusion: peripheral nerve retrograde transport of a neurotoxin targets motor neuron survival and motor function*

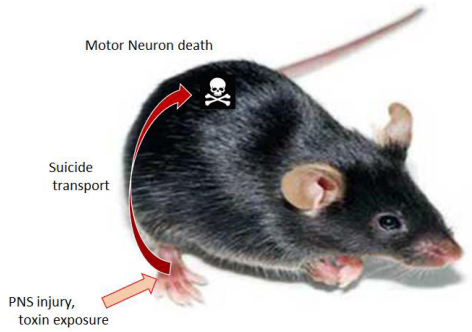

Abstract

We describe a pre-clinical spinal cord motor neuron injury model that is minimal invasive, reproducible, focal and easily applied to small rodents. Retrograde axonal transport of a pro-apoptotic phosphatidylinosotol 3'-kinase inhibitor, wortmannin, via the sciatic nerve results in loss of ipsilateral lumbar motor neurons proportional to the level of drug administered. Motor neuron loss was detected by choline acetyltransferase (ChAT) immunostaining and with a transgenic thy1-*eGFP* marker. The short half-life of wortmannin generates minimal wound spread, and wortmannin does not affect axon transport, as determined by co-injection of a pseudorabies virus tracer. Using quantitative transcript analysis, we found that *ChAT* transcripts significantly decreased at 14 days post-delivery of 1 µg wortmannin, relative to sham controls, and remained low after 90 days. Smaller effects were observed with 200 ng and 100 ng wortmannin. Wortmannin also generated a transient and significant increase in astrocyte *Gfap* transcripts after 14 days with a return to control levels at 90 days. Treated mice had hind limb spasticity and a forced motor function defect that was quantified using a water exit test. Controls rapidly exit a shallow water tray, and wortmannin treated animals were up to 12-fold slower, a phenotype that persisted for at least 3 months. Thus the focal delivery of wortmannin to motor neurons generates a reproducible and scalable injury that can facilitate quantitative studies on neural regeneration and repair. The efficacy of sciatic nerve suicide transport can also explain neurotoxin-mediated selective loss of motor neurons in diseases such as amyotrophic lateral sclerosis. All procedures were performed at Rutgers under established Institutional Animal Care and Use protocols (eIACUC_TR201800022, approved on March 20, 2018).

Key Words: amyotrophic lateral sclerosis; injury; motor function; motor neuron; PI3'kinase; sciatic nerve; suicide transport; wortmannin

Chinese Library Classification No. R453; R364; R741

Introduction

Neurotoxicity and neurotrauma present significant challenges for clinical medicine and are a major focus of drug development and basic research. As with all clinical challenges, novel therapeutic approaches that drive clinical trials are dictated by progress in basic research using animal models. However, for brain and spinal cord insults, the complexity of traumatic injury models (Cheriyan et al., 2014; Kjell and Olson, 2016; Dietz and Schwab, 2017; Minakov et al., 2018) introduces experimental variability and led to calls for revised approaches in experimental design (Lemmon et al., 2014; Snow, 2014). Here we consider the premise that studies on neural regeneration and repair could benefit from less complex experimental models.

A trauma free approach to generate a motor neuron insult is toxin delivery via peripheral nerve suicide transport (Wiley et al., 1982). This strategy has been used to deliver ricin (Harper et al., 1980; Yamamoto et al., 1985; Wiley and Oeltmann, 1986; Liang et al., 2018), a broad scale toxin that generates both peripheral and central nerve damage and mortality. Here we show that retrograde suicide transport of a pro-apoptotic compound, the phosphatidylinositol 3'-kinase (PI3K) inhibitor wortmannin, results in focal loss of ipsilateral motor neurons without blood brain barrier breakdown, necrotic cell

[1]Department of Neurosurgery, Rutgers-Robert Wood Johnson Medical School, Piscataway, NJ, USA; [2]Member, The Cancer Institute of New Jersey, New Brunswick, NJ, USA

***Correspondence to:** Randall D. McKinnon, PhD, mckinnon@rwjms.rutgers.edu.

https://orcid.org/0000-0002-7539-9613 (Randall D. McKinnon)

Funding: *Supported by grants to Dr McKinnon (PI) from the New Jersey Commission on Spinal Cord Research (05-3047; 11-015).*

How to cite this article: *Liang AS, Pagano JE, Chrzan CA, McKinnon RD (2021) Suicide transport blockade of motor neuron survival generates a focal graded injury and functional deficit. Neural Regen Res 16(7):1281-1287.*

death, or lethality. The surgical model is straightforward, the extent of injury is dose-dependent, and the injury generates a sustained forced motor function defect that can serve as a reliable measure for the efficacy of neural regeneration and repair strategies. Thus wortmannin suicide transport presents a reproducible model that can facilitate large scale pre-clinical studies. The efficacy of toxin delivery via peripheral nerves also supports the hypothesis that suicide transport underlies the etiology of acquired motor neuron diseases such as ALS (Yamamoto et al., 1985).

Materials and Methods

Reagents and drugs

Wortmannin was obtained from Sigma (St. Louis, MO, USA) and Chir 99021 (an inhibitor of the Wnt signaling pathway) from Stemgent (Cambridge, MA, USA). Stock solutions (1 mM) in dimethyl sulfoxide (DMSO) were stored at –80°C and diluted in phosphate buffered saline (PBS) to a working concentration (100 ng/μL) immediately before use. Plasmid vector pCMV-*eGFP-N 1* was from Clontech (www.takarabio.com), synthetic polymerase chain reaction (PCR) primers were from Integrated DNA Tech (www.IDT.com), pseudorabies virus viral stocks (PRV-152; PRV-614) were prepared as described (Card and Enquist, 2012), and mesenchymal stromal cells (MSC) were isolated as previously described (Arriola et al., 2010). Rabbit anti-choline acetyltransferase (ChAT) was from Sigma, rabbit anti-glial fibrillary acidic protein (GFAP) from Chemicon (Temecula, CA, USA), rabbit anti-Iba1 from Wako Ltd (Osaka, Japan), and all other monoclonal antibodies from the Developmental Studies Hybridoma Bank (Univ. Iowa, Iowa City, IA, USA). Alexa Fluor conjugated secondary antibodies were from Molecular Probes (www.thermofisher.com). C57BL/6J mice (both wild-type and strain B6.Cg-Tg(Thy1-YFP)HJrs/J) were from Jax Labs (Bar Harbor, ME, USA).

Sciatic nerve injury

All procedures were performed at Rutgers under established Institutional Animal Care and Use protocols (eIACUC_TR201800022, approved on March 20, 2018), with the sciatic nerve (Sn) accessed as previously described (Savastano et al., 2014). This study includes analysis of three independent cohorts (n = 20, 25, and 56, respectively) of mixed gender adult C57BL/6J mice (body weight ~20–25 g) with long-term surgical survival of 97% (two mice died during anesthesia). Wild-type mice were not surgical, and sham controls received 1 μL of vehicle only (PBS, 0.2% DMSO). All drug deliveries described involve injections into the left Sn at mid-thigh level. Briefly, mice were anesthetized by intraperitoneal injection with 0.1 mL/10 g of a freshly prepared solution containing 100 mg/mL ketamine and 10 mg/mL xylazine. The thigh fur was cleaned with 70% ethanol, a 3 cm incision through the skin exposed the underlying muscle layers which were gently separated to expose the proximal Sn, and then the nerve was lifted onto the flat side of sterile scissors resting on the surgical field. A Hamilton syringe was used to deliver a 1 μL bolus into the nerve sheath with the needle bevel oriented inward. The bolus was slowly injected over 60 seconds and the needle withdrawn after another 30 seconds to allow the fluid to disperse in the nerve. DMSO was included in the bolus to facilitate axon penetration. After injection the nerve was repositioned between muscle groups, the skin incision closed with surgical thread, and the animals were placed under a heat lamp until they recovered from the anesthesia. The entire procedure can routinely be completed in 10 minutes per nerve.

Histological analysis

Anesthetized animals were cardiac perfused with PBS followed by PBS containing 4% paraformaldehyde. After overnight fixation the spinal column and attached peripheral nerves were dissected for whole mount analysis. Since mouse spinal cord segments do not align with the vertebral landmarks (Harrison et al., 2013), this dissection approach allowed for unambiguous assignment of cervical (Cv), thoracic (Th), lumbar (Lu) and sacral spinal cord segment boundaries. The vertebrae were removed using 6 × 0.15 mm micro-dissection scissors (Roboz, Gaithersburg, MD, USA), then for orientation we used a 25-gauge needle to embed Mallinckrodt 4932 inert charcoal (Wasatch Chem, Salt Lake City, UT, USA) into the right spinal cord segments. For vibratome sectioning the spinal column was embedded in 0.3% agarose. Individual sections (100–200 μm) were washed in PBS containing 0.1% triton X-100 (PBT) then incubated with primary antibodies in PBT for at least 48 hours at 4°C. Controls included no primary as well as non-target antibodies. The sections were then extensively washed in PBT (two washes each at room temperature for 30 minutes, one each at 4°C overnight) then exposed to fluorescent conjugated secondary antibodies at room temperature for 4–6 hours. Sections were then washed as above and mounted in Vectashield H-1200 (Vector Labs, Burlingame, CA, USA) on Lab-Tek 155360 chambered cover glass slides (Sigma). For low magnification photography, we used a Zeiss Axiovert TM100 fluorescent microscope (10× objective) and for high resolution we used a Zeiss LSM confocal with 25× and 63× water emersion objectives. Fluorescent images were collected at 1 μm z-plane intervals and selected planes merged by projection using LSM Image Browser software (www.zeiss.com). A panel labeled Z1-25@3 represents a compilation of every 3rd image from a 25 μm z-stack. Image montages were assembled using Adobe Photoshop, vr Elements 2019 (www.adobe.com).

Quantitative RT-PCR analysis

We used reverse transcriptase (RT) followed by quantitative polymerase chain reaction (PCR) to measure relative transcript levels. Tissue was harvested (n = 2 animals per experimental group) after cardiac perfusion with cold PBS (4°C) followed by isolation of the spinal column as outlined above. The peripheral nerves, including proximal Sns, were retained to ensure proper boundary assignment of cord segments (Harrison et al., 2013) during the subsequent dissection. First the dorsal cord, from dura to the central canal, was split along the entire midline, and then the ventral cord was teased apart along the entire ventral midline. The left and right hemi-cords were then cut into eight tissue block sections including one Cv, three Th, three Lu and one sacral. The dura and peripheral nerves were then removed from each section using Roboz RS-5045 forceps (www.roboz.com), and each tissue was immersed in Trizol (Gibco, www.thermofisher.com) for RNA isolation following the manufacturer's instructions. The RNA was dissolved in 50 μL of sterile H_2O and a 1 μL aliquot was reverse transcribed into first strand complimentary DNA (cDNA) using Gibco RT following the manufacturer's instructions.

For qPCR the cDNA was diluted 1:10 in sterile H_2O then aliquots assayed using gene specific primer pairs (www.IDTDNA.com) and Power Sybr Green reagent (Applied Biosystems, Foster City, CA, USA) in triplicate wells on a 96 well plate in a BioRad CFX Connect real time PCR thermocycler. The forward (f) and reverse (r) PCR primers include: *Gapdh* 447f: 5′-AGC CAA AAG GGT CAT CAT CTC, *Gapdh* 643r: 5′-CTG TGG TCA TGA GTC CTT CCA; *ChAT* 1236f: 5′-CCA GAA ACT CAA GGC CAT CT, *ChAT* 1726r: 5′-CGG TTG CTC ATC AGG TAT GT; *Gfap* 523f: 5′-GCA GAA GCT CCA GGA TGA AAC CAA, *Gfap* 643r: 5′-GCG ACT CAA TCT TCC TCT CCA G. Each qPCR assay included triplicates of tissue cDNA samples with test primers (*ChAT*, *Gfap*) and primers to detect an internal control transcript, *Gapdh*, to normalize for the amount of tissue represented in different samples. The average threshold value (C_T, at a baseline of 1000 relative light units) was normalized to *Gapdh* (delta C_T) for each cDNA sample. This ratio was then compared to the same ratio from control mice to generate (delta-delta C_T) and calculate relative levels (R_Q) (Livak, and Schmittgen, 2001). We calculated R_Q in parallel tissue samples from non-

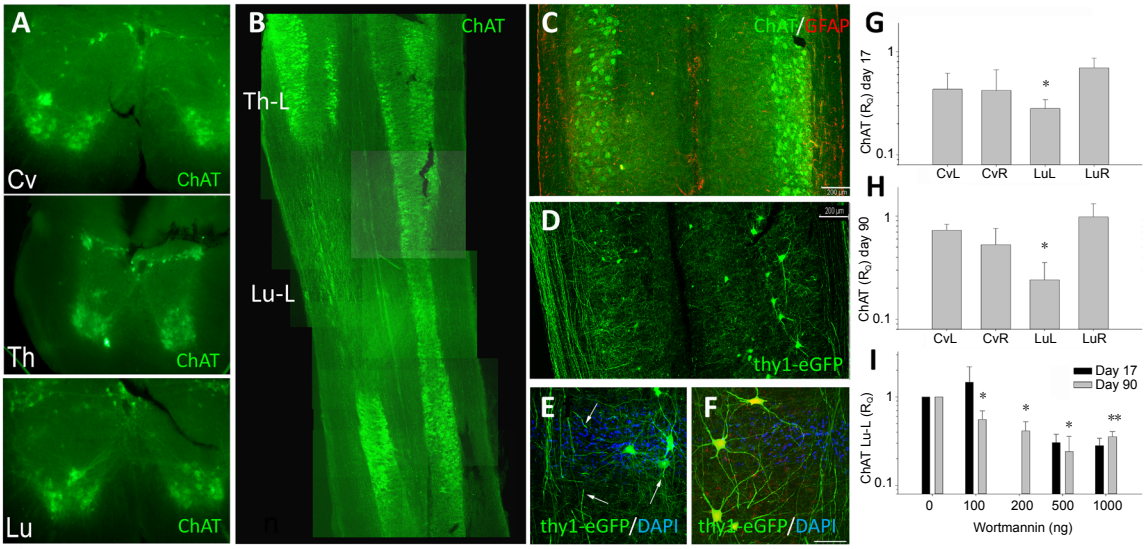

Figure 1 | **Spinal cord motor neurons in mice on the indicated day after injecting wortmannin (Wmn) into the left Sn (Sn-L).**
(A) Wild-type control mice; ChAT+ motor neurons (green fluorescence) in cervical (Cv), thoracic (Th) and lumbar (Lu) spinal cords. Axial view, dorsal is top. (B) ChAT after 30 days, 1000 ng Wmn; dorsal view, anterior is top. Merged confocal images from one 80 µm section at 3 µm Z-axis projections. (C) High resolution of the ventral cord (30 days, 100 ng Wmn). Fluorescence signals are (green) $ChAT^+$ motor neurons and (red) $GFAP^+$ astrocytes; dorsal view, anterior is top. (D) Lumbar (Lu5–6) spinal cord of *thy1-eGFP* mice (4 days, 100 ng Wmn). Fluorescence signals are (green pseudo color) YFP^+ motor neurons, and (blue) nuclear DAPI; dorsal view, anterior is top, and Z-axis spans 23 µm at 3 µm intervals. (E, F) High magnification of (D) showing left and right lumbar cord; dorsal view, anterior is top, and Z-axis spans 5 µm. Arrows in panel E show axonal pathology. Scale bars: 200 µm in A–D and 100 µm in E, F. (G) Threshold qRT-PCR analysis (R_Q) of *ChAT* transcripts in left and right Cv and Lu cord sections (17 days, 100 ng Wmn). The C_T^{ChAT} in each sample was first normalized to C_T^{Gapdh} then expressed relative to the same ratio in vehicle only control animals. (H) *ChAT* transcript levels (90 days, 100 ng Wmn) as in G. (I) *ChAT* in Lu-L cord, 17 and 90 days after injecting the indicated dose (ng) of Wmn into the left Sn; 0 ng, vehicle only control. Results (mean ± SD) are from $n = 4$ independent samples assayed in triplicate. Student's *t*-test: $^*P < 0.05$, $^{**}P < 0.001$.

surgical and vehicle only (DMSO) control mice.

Motor function

Wortmannin-treated animals appeared normal while free roaming but displayed left hind leg spasticity when elevated by the tail. To quantitate this, we measured exit times from a shallow water tray (Kiel et al., 2008). To minimize distractions and stress all water exit tests were performed at the same time, twice daily, within the animals' home cage and familiar housing. Individual animals were bar coded prior to surgery, experimenters were blinded for all tests and hind limb phenotypes were not obvious during handling. An 8 cm × 10 cm × 4 cm tray containing room temperature water (depth 0.5 cm) was placed in the home cage, then individual animals were gently placed in the center of the tray and the time required to return their front feet to the cage bedding was recorded. At least seven consecutive measurements were taken and we calculated the sequential cumulative time. Results are presented as the cumulative average of the sequential tests for all cohorts, grouped into three time points (days 4–5, days 6–10, and > 10 days) post-surgery. The longest time point examined was 90 days. This sequential sum allowed for test time variations such as early exit "popping out" or delayed exit from fatigue, with an upper limit of 300 seconds used for animals that did not descend from the tray edge. While individual times varied, the cumulative average for individual animals in each test condition were remarkably stable and produced large and statistically significant differences (from 10 to 100-fold) between experimental groups.

Statistical analysis

Statistics including two-tailed Student's *t*-test were performed using SigmaPlot version 13 (Systat Software Inc., San Jose, CA, USA), with Mann-Whitney post hoc analysis, to assess normal distribution of data and the significance between control and experimental test groups. A value of $P < 0.05$ was considered the threshold for statistical significant difference.

Results

Sciatic nerve delivery of wortmannin depletes spinal cord motor neurons

We examined the potential for retrograde transport (Wiley et al., 1982) via the Sn to deliver wortmannin and target the destruction of trophic factor dependent lumbar spinal cord motor neurons (MN). Wortmannin is a covalent inhibitor of PI3K, a key intermediate in the survival signaling pathway for of trophic factor dependent cells. Wortmannin binds the PI3K catalytic domain (Walker et al., 2000), blocks activity at very low concentrations (IC_{50} = 5 nM), and it has a short half-life (10 minutes) due to instability of the C_{20} carbon that covalently inactivates PI3K. To determine the effects of wortmannin on MN, we examined the expression of the motor neuron marker ChAT in drug treated (1000 ng) and vehicle only control animals. The targeted MN pools reside in ventral lateral horns of the lumbar spinal column (**Figure 1A**).

Using histochemistry, ChAT immune staining after wortmannin treatment revealed a dramatic and focal reduction in the ipsilateral (left) MN pool (**Figure 1B** and **C**). There was no obvious loss of ChAT in segments either rostral or caudal to this Sn entry zone, or at any level of the contralateral spinal cord (**Figure 1C**). We also examined wortmannin effects using *thy1-YFP* transgenic mice that express the Yellow Fluorescent Protein marker in MN. YFP identified MN soma and their processes extending laterally and into longitudinal axonal tracts (**Figure 1D**). Four days after injecting wortmannin into the left Sn, there was a focal reduction of ipsilateral lumbar level (Lu1–6) MNs (**Figure 1D**) with surviving MN showing less YFP expression and lateral processes. High resolution revealed blebbing and discontinuities in longitudinal axons (**Figure 1E**, arrows). None of these defects were observed distal to the left lumbar Sn entry zone, or in the contralateral spinal cord at any level (**Figure 1F**). After 17 days, there was no evident increase in this focal MN loss, suggesting the short half-life of wortmannin limits its effect to transient MN damage in the lumbar cord.

We extended these qualitative studies with a quantitative

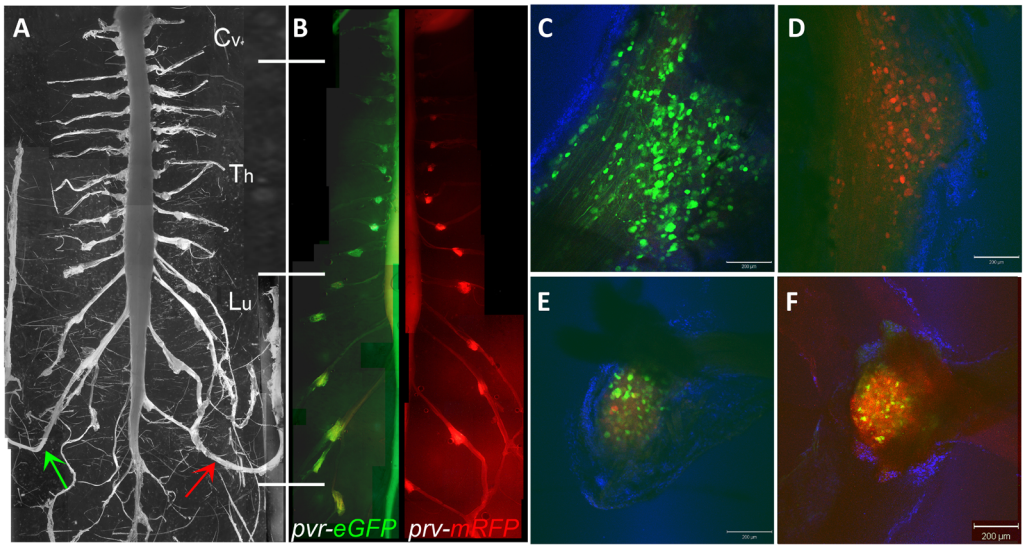

Figure 2 | Retrograde transport after wortmannin delivery to the sciatic nerve.
On day 0 mice received wortmannin in the left sciatic nerve, on day 2 they received PRV-*eGFP* in the left sciatic nerve (green arrow) and PRV-*mRFP* in the right sciatic nerve (red arrow), then were harvested on day 6. (A) Phase contrast and (B) fluorescent image montage of the cervical (Cv) thoracic (Th) and lumbar (Lu) spinal cord and peripheral nerves. Dorsal view, anterior is top. (C, D) Expression of eGFP and mRFP in sciatic nerve dorsal root ganglia. (E, F) Co-expression of eGFP and mRFP in thoracic dorsal root ganglia. Scale bars: 200 µm in C–F.

biochemical approach using qRT-PCR analysis of ChAT transcripts in whole cord tissue sections (**Figure 1G–I**). This analysis again revealed significant loss of *ChAT* in the ipsilateral lumbar left (Lu-L) cord at both 17 days (**Figure 1G**) and 90 days (**Figure 1H**) after 1 µg wortmannin delivery. On day 17 the *ChAT* transcripts in the Lu-L were 80% lower than in the wild-type mice (0.18 ± 0.09) and 70% lower than in vehicle only control animals (0.28 ± 0.06), and the difference was statistically significant ($P < 0.05$). On day 90 the *ChAT* transcripts in Lu-L remained well below both wild-type (0.13 ± 0.02) and vehicle controls (0.35 ± 0.05, **Figure 1H**), and these differences were again significant ($P < 0.01$). Wortmannin did not decrease *ChAT* transcript levels in the contralateral lumbar right (Lu-R) cord (0.77 ± 0.25, $P = 0.533$) or in the cervical cord (Cv-L: 0.49 ± 0.03, $P = 0.28$; Cv-R: 0.53 ± 0.23, $P = 0.35$), compared to the same cord segments in vehicle only control animals. Again this was consistent with a transient injury due to the short half-life of wortmannin, and further indicated that MN loss was not repaired within the longer time frame.

We also detected a dose dependence on *ChAT* levels in the ipsilateral lumbar cord (**Figure 1I**). *ChAT* levels with 100 ng wortmannin were 34% lower than vehicle controls (0.56 ± 0.14, $P < 0.05$), they were 60% lower with 200 ng wortmannin (0.41 ± 0.1, $P = 0.13$), and 65% lower with 1 µg (0.35 ± 0.05, $P < 0.01$). *ChAT* levels in the Lu-L cord of vehicle controls were not significantly different from wild-type mice at either 17 days ($P = 0.3$) or 90 days ($P = 0.12$) post-surgery. Together these results indicate that Sn delivery of wortmannin results in a dose-dependent focal loss of MN in the ipsilateral lumbar spinal cord.

Wortmanin does not disrupt retrograde transport

For wortmannin to induce MN cell death it must enter the Sn axons then move into their soma in the central nervous system (CNS). DMSO in our injection bolus should allow axon penetration in the nerve, and the trauma of injection should promote reverse axonal transport (Bisby and Bulger, 1977) as seen with transport of lectins injected into peripheral nerves (Wiley et al., 1982). However, it was possible that wortmannin could block retrograde transport or cause damage within the peripheral nerve, as reported after ricin delivery (Liang et al., 2018), with MN loss being an indirect secondary effect. To examine this, we used pseudo-rabies virus axonal tracers that encode transgenic markers including green (PRV-*eGFP*) and red (PRV-*mRFP*) fluorescent proteins. PRV virions undergo selective retrograde transport and are excellent tracers for mapping trans-synaptic axonal connections (Card and Enquist, 2012).

We first injected wortmannin into the left Sn, then after 48 hours we injected PRV-*eGFP* into the left and PRV-*mRFP* into the right Sn and monitored viral spread in whole mount preparations (**Figure 2**). The results observed in wortmannin treated animals were identical to the vehicle only control mice. Marker expression on day 6 was evident at all spinal column levels (**Figure 2B**), with eGFP prominently in the left and mRFP prominently in right dorsal root ganglia (DRG). In the Sns the markers were restricted to the respective left and right axons and associated DRG. mRFP was absent from the left Sn DRG (**Figure 2C**), and eGFP was absent from the right Sn DRG (**Figure 2D**). In the thoracic DRG in contrast, there was approximately 10% crossover of mRFP into the left (**Figure 2E**) and eGFP into right (**Figure 2F**). Thus pre-treatment of the left Sn with wortmannin did not block subsequent retrograde axon transport of PRV-*eGFP*. Assuming wortmannin accesses the same axons and transport vesicles as PRV virions, this is consistent with the interpretation that wortmannin can reach the ventral spinal cord via Sn retrograde transport to modulate MN survival.

Sciatic nerve insult generates transient reactive gliosis in the CNS

We next asked whether injection of wortmannin into the Sn generated reactive gliosis in the spinal cord, a prominent signature of CNS injury. Using histochemistry we detected robust expression of the astrocyte marker GFAP after 3 days in wortmannin-treated mice (**Figure 3A–C**). The gliotic response was focal and localized to the ipsilateral lumbar cord (Lu-L), proximal to the Sn entry zone (**Figure 3A**). Increased levels of GFAP were not detected in control mice, and we did not observe reactive astrocytes at earlier time points post wortmannin suggesting that gliosis was subsequent to the wortmannin-induced MN injury. The gliotic response persisted in the ipsilateral Sn entry zone at 5 weeks post wortmannin and spread into the contra-lateral cord (**Figure 3B**). High resolution demonstrated reactive astrocytes within the spinal cord parenchyma in integral contact with longitudinal motor neuron axonal tracks (**Figure 3C**).

Quantitative RT-PCR analysis also demonstrated a dose-dependent increase in *Gfap* transcripts 17 days after wortmannin injection (**Figure 3D** and **E**). Thus *Gfap* transcripts proved to be a sensitive indicator of wortmannin effects. Relative to vehicle only control animals, *Gfap* transcripts in the ipsilateral lumbar cord increased by 21 ± 4-fold after 100 ng wortmannin, and 268 ± 87-fold with 500 ng wortmannin, and these differences were significant ($P < 0.001$). This analysis also showed a smaller increase relative to controls in the contralateral lumbar cord (1.9 ± 0.8), as well as in the

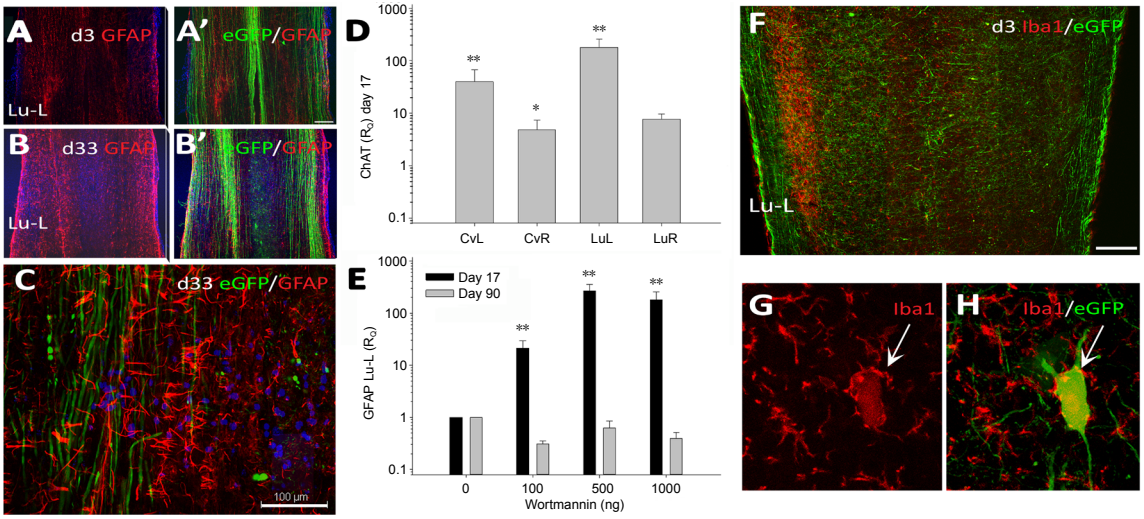

Figure 3 | **Wortmannin (Wmn)-induced glial response in the lumbar spinal cord on the indicated days after injecting Wmn into the left sciatic nerve of *thy1-YFP* mice.**

(A, A') Astrocyte gliosis in the lumbar left (Lu-L) spinal cord (3 days, 100 ng Wmn); fluorescence signals are (red) GFAP$^+$ astrocytes, (green pseudo color) YFP motor neurons, and (blue) nuclear DAPI. (B, B') Astrocyte gliosis (33 days, 100 ng Wmn), as in panel A. (C) High resolution of panel B. (D) Threshold qRT-PCR (R_Q) of *Gfap* transcripts in left and right cervical (Cv) and lumbar (Lu) spinal cord sections (17 days, 100 ng Wmn). The C_T^{Gfap} in each cord sample was normalized to C_T^{Gapdh} then expressed relative to this ratio in vehicle only controls. R_Q values were from (top panels) $n = 4$ animals and (bottom) duplicate cDNA preparations from individual animals. Student's *t*-test: $^*P < 0.05$, $^{**}P < 0.001$, *vs.* vehicle controls. (E) *Gfap* transcripts in Lu-L spinal cord (17 and 90 days, 100 ng Wmn), as in panel D. (F) Microglia in the lumbar left (Lu-L) spinal cord of *thy1-YFP* mice (3 days, 100 ng Wmn); fluorescence signals are (red) Iba1$^+$ microglia and (green pseudo color) YFP$^+$ motor neurons. (G, H) Microglial processes (arrow) enwrap a YFP$^+$ motor neuron. All images show dorsal view with anterior at top. Z-axis projections: 27 µm in A and B; 36 µm in C; 12 µm in F; 66 µm in G and H. Scale bars: 200 µm in A, A', B, B', F and 100 µm in C, G, H.

left (12.7 ± 4.0) and right (5.8 ± 0.7) cervical cords, and these differences were also significant ($P < 0.05$). Interestingly, after 3 months the *Gfap* levels were not significantly different than control levels (**Figure 3E**). Thus wortmannin generated a transient focal gliosis in the spinal cord, in contrast to the stable focal effects on ipsilateral MNs.

We also observed a transient microglial response that was qualitatively similar to reactive astrogliosis. At 72 hours post injection there was a focal increase of the microglial marker Iba1 in the ipsilateral lumbar spinal cord (**Figure 3F**). These microglia had ramified processes that appeared to enwrap MN soma (**Figure 3G** and **H**), consistent with an active phagocytic response. Together these observations indicate that Sn delivery of wortmannin results in rapid, focal and transient spinal cord gliosis in the Sn entry zone.

Forced motor activity

Very shortly after wortmannin delivery the mice consistently developed a spastic left hind limb that was not seen in sham surgery animals. This was easily observed upon elevation by the tail, although when free roaming these animals showed no obvious deficit. To examine their locomotor skill, we measured the time required for animals to exit a water tray (Kiel et al., 2008). Wild type C57BL/6J mice exited the water without hesitation (2.1 ± 0.8 seconds) with no difference between gender, age or body weight. There was no obvious sign of fatigue and cumulative times after 7 consecutive tests, averaged over multiple days, was 18 ± 7 seconds (**Figure 4A**). C57BL/6J mice which received wortmannin, in contrast, were slower to initiate motor activity and frequently paused. Mice that received 100 ng wortmannin had a cumulative time of 452 ± 170 seconds and the difference from both wild-type (non-surgical) and sham controls (vehicle injection only) was significant ($P < 0.01$). Mice from a second independent wortmannin treatment cohort had similar exit times (433 ± 192 seconds, $P < 0.001$). This cumulative sum proved to be a quantitative and statistically significant measure of differences (10 to 100-fold) between experimental treatments.

A small component of this motor defect appeared due to the hind limb surgery alone, as sham surgery (vehicle only) animals had cumulative exit times of 37 ± 21 seconds (**Figure 4A**), significantly slower than wild type mice ($P = 0.0004$). These sham surgery effects are consistent with acute neuronal pathology including reversal of axonal transport (Bisby and Bulger, 1977) while the slower times after wortmannin delivery are consistent with MN loss. Of note, animals where we surgically removed a 4 mm section of the left Sn were not significantly different from vehicle only sham control mice (53 ± 20 seconds, $P = 0.166$, $n = 5$ mice, 40 trials). Wiley and Oeltmann (1986) previously reported that the destruction of motor neurons generates a more dramatic phenotype than complete axonal transection.

The motor deficit was not evident for the first 5 days after surgery, with no obvious differences between wortmannin (27 ± 12 seconds, $P = 0.138$) and the sham surgery injection groups. The motor deficit phenotype emerged from 6–10 days post treatment (125 ± 48 seconds, 42 trials), stabilized after 10 days (452 ± 170 seconds), and for both test periods the differences between wortmannin-treated ($P = 0.034$, 289 trials) and vehicle only controls were significant (**Figure 4B**). This level of motor defect persisted through 3 months, the longest time point examined. Thus the forced motor score proved to be a quantitative and sensitive measure of motor neuron loss, consistent with a transient injury generating a stable defect.

Finally, we examined the relationship between drug dose and motor function (**Figure 4C**). We compared the effects of wortmannin doses from 100 ng to 4 µg, and examined each condition at (i) 4–5 days, (ii) 6–10 days, and (iii) > 10 days post-surgery. Relative to the vehicle controls, there were no differences in any wortmannin dose during the first 4–5 days post-surgery (**Figure 4C**, group i). For each wortmannin doses tested there was a significant increase in exit times from 6–10 days (**Figure 4C**, group ii), and again after 10 days (**Figure 4C**, groups iii). However, there was no evidence for an increase in exit times at higher amounts of wortmannin. For the day 10+ group (iii) the exit times were not significantly different for mice treated with 100 ng (433 ± 191 seconds), 200 ng, 500 ng, 1000 ng and 4000 ng. Similar results were observed for the day 6–10 (group ii) tests (**Figure 4C**). This lack of dose-dependent motor phenotype was very distinct from the effect of wortmannin dose on ChAT histochemistry

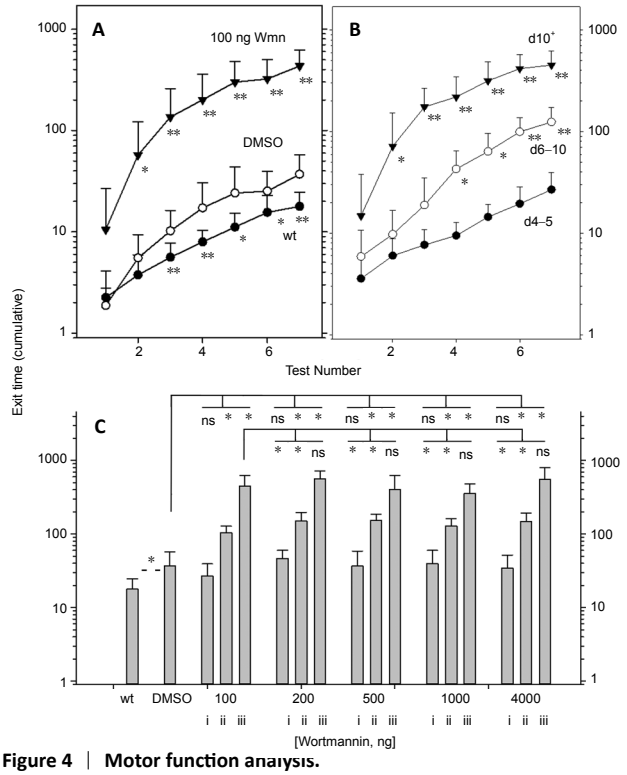

Figure 4 | **Motor function analysis.**
(A) Cumulative exit times (seconds) after each of seven consecutive tests for wild-type mice (wt) and mice injected in Sn-L with vehicle control or 100 ng wortmannin (Wmn). (B) Cumulative exit times at the indicated test days after injecting Sn-L with 100 ng Wmn. (C) Cumulative times of seven tests at (i) 4–5 days, (ii) 6–10 days, and (iii) >10 days after injecting Wmn into Sn-L. Number of cohorts: wt (8 mice, 55 trials), vehicle (5 mice, 155 trials), 100 ng Wmn (7 mice, 58 trials; 6 mice, 131 trials), 200 ng Wmn (3 mice, 35 trials), 500 ng Wmn (7 mice, 139 trials), 1000 ng Wmn (4 mice, 111 trials), 4000 ng Wmn (4 mice, 49 trials). Data are expressed as the mean ± SD. *P*-values (**P* < 0.05, ***P* < 0.01) probability the results differ by chance from (A, B) vehicle only and (C) 100 nM Wmn (Student's *t*-test).

and transcript levels under these same conditions (**Figure 1**). This may suggest that retrograde transport via the Sn delivers wortmannin to a subset of MN, though this remains to be determined.

Motor phenotype rescue

We next used forced motor function to examine other aspects of Sn mediated motor neuron injury. To ask whether the wortmannin effects were drug specific we used a distinct pharmacological agent (Chir 99021), an inhibitor of the Wnt signaling pathway (**Table 1**). The motor function of these mice (131 ± 45 seconds) was closer to sham control than wortmannin injected mice, and the differences for each (*P* < 0.05) were significant. We also used motor function to explore the potential of stem cell grafts as a therapeutic approach to prevent injury spread (**Table 1**). Mice received 1 µg wortmannin via Sn injection, and then on day 7 received either MSC or vehicle only (PBS) into the delaminated lumbar spinal cord. Exit times for the control group (Sn-Wmn::SC-PBS) were comparable to the mice that only received wortmannin via Sn delivery, and to mice that received wortmannin via direct SC injections (SC-Wmn, **Table 1**). In contrast, for 50% of the animals which received MSCs (Sn-Wmn::SC-MSC), exit times were significantly faster than the controls (75 ± 23, *P* < 0.01, **Table 1**). Further analysis is required to determine whether this may represent an attenuation of either MN loss or immune response.

Reproducibility of sciatic nerve delivery

We also used motor function to examine the efficacy of Sn suicide transport. In control groups, including Sn injections of vehicle and injections of Chir 99021 (**Table 1**), 88% (7/8) had a mild motor phenotype while one mouse had an apparent injury with significantly slower exit time (106 ± 15 seconds, *P* = 0.001). In Sn wortmannin studies, there were three independent surgical groups. In initial studies using low levels of wortmannin (40–80 ng), 56% of the animals (9/16) had a significant motor function defect while the remainder were comparable to sham controls. At least some of these apparent failures may represent a learning curve for drug delivery, since 100% of animals in the two subsequent cohort studies (24/24, > 100 ng wortmannin) had significant motor deficits. We did note that Sn delivery of the highest dose (4 µg) was somewhat compromised by the viscosity of the delivery solution. Overall, these results demonstrate that Sn delivery of wortmannin generated a remarkably consistent and reproducible focal motor neuron injury and functional defect.

Table 1 | **Forced motor function**

Treatment	Test day	Exit time (s)	Number of mice	Number of trials	*P*-value
Wild-type	–	18±6.8	8	55	0.0004
Sn-PBS	4–10+	37±21	5	155	*
Sn-Chir 99021	6–10+	131±45	2	40	0.018
Sn-Wmn::SC-PBS	10+	244±149	4	49	0.001
Sn-Wmn::SC-MSC	7–15+	75±23	3	12	0.00013
SC-Wmn	10+	227±108	2	74	0.007

Cumulative water tray exit time after seven consecutive trials (seconds, mean ± SD) after the indicated treatments into the left sciatic nerve (Sn-L) or the dorsal thoracic spinal cord (SC). Wmn: 100 ng wortmannin. Results are from the indicated number of mice and total trials per group. (*P*) Students' *t*-test probability that results differ by chance from vehicle treated controls (*).

Discussion

Wortmannin delivery into the proximal Sn generates a reproducible lumbar spinal column motor neuron injury that can be reliably quantified using a simple forced motor function test. The Sn surgical procedure is minimal invasive, can accommodate large sample sizes, post-operative recovery is rapid and survival is 100%. The wortmannin induced phenotype was not seen after sham injection surgery or with other types of Sn insults, including viral (PRV-*eGFP*) delivery into the nerve or complete Sn transection. Wortmannin also did not disrupt short term retrograde axonal transport, indicating that it can reach the thoracic spinal column to affect motor neuronal survival. Peripheral nerve transport may also be useful for delivery of agents, such as cuprizone mediated demyelination, and as a model for studies on experimental approaches to promote neural regeneration and repair.

The short half-life of wortmannin (10 minutes) suggests its effects would be restricted to the first cells that encounter the drug. Assuming retrograde transport from injection site to the thoracic spinal cord, a distance of approximately 15 mm, this would yield an effective dose of 200 pg active drug in the ventral cord. This would be sufficient to initiate MN cell death, since in prior studies induction of cell death required an ED_{50} of 10 nM (4 pg/µL) wortmannin (Ebner et al., 2000). The wortmannin induced injury was distinct from trauma induced wounds, which more closely model clinical cases of traumatic spine injury, in that it did not alter bone, muscle or blood vessels. It did generate a loss of motor neuron axons and soma, and a significant gliotic response including activated microglia and astrocytes in the vicinity of Sn entry points in the cord. It remains to be determined whether this gliotic response is a result of motor neuron death or a secondary response to the wortmannin induced injury. We did not see any indication of parenchymal cavitation that is a hallmark of traumatic cord injury in rodents, suggesting the wortmannin injury is similar to secondary damage by neurotoxicity subsequent to trauma induced neuronal death (Cheriyan et al., 2014).

Motor function was examined using a simple, cost effective and sensitive water avoidance test that has proved to be both reliable and consistent (Kiel et al., 2008). This test easily distinguishes between control, sham surgery and drug-treatment groups, and the scale of response times in this test is logarithmic, a sharp contrast to the linear differences in results from other tests used for motor function. To date we have not compared this to other tests such as the Basso Beattie Bresnahan locomotor rating scale (Basso et al., 1995), Kinematics scales (Hillyer and Joynes, 2009) or the staircase test (Okabe et al., 2017). We examined adult mice of mixed gender and age, and of note DBA mice proved less reliable than C57BL/6J as they seemed less motivated to exit the water tray. Since the most affected animals tended to rest on the top corner of the tray at later stages of individual testing periods, we set an upper limit of 300 sec for any one timed run to avoid skewing the results. We also excluded individual times that were ±2 standard deviations from the mean. The exclusion frequency increased with severity of motor impairment, with 2% for wild-type animals, 10% for surgical control groups and 5% for wortmannin-treated animals.

Retrograde "suicide transport" of cytotoxic lectins has been used previously to eliminate CNS neuronal populations (Wiley et al., 1982). Other chemical models used for spine injury include less targeted systemic delivery strategies such as photochemical ischemia (Watson et al., 1986), neurotransmitter excitotoxicity (Liu et al., 1999), reactive oxygen toxicity (Bao and Liu, 2002), pro-inflammation (Liu et al., 2006) and chemical demyelination (Cheriyan et al., 2014). Our use of a transiently stable toxin with a very short half-life represents an important extension of suicide transport, as cytotoxicity is limited to the first neurons that encounter the drug. We have not examined whether Sn-wortmannin generates a hyperalgesic response to pain stimuli or sensitization to otherwise innocuous stimuli (allodynia). It will also be of interest to test whether wortmannin delivery into forelimb nerves (Wiley and Oeltmann, 1986) affects cervical motor neurons, and whether retrograde transport can be used to protect motor neurons or promote their repair by therapeutic drug delivery.

The selective death of MNs by retrograde transport of toxins was previously proposed to explain the etiology of human motor neuron degenerative diseases (Yamamoto et al., 1985). While a small number of genes have been associated with predisposition to MND (Bruijn et al., 2004), 90% of ALS cases to date are "sporadic" with no known genetic linkage and one of the strongest risk factor to date is exposure to agricultural pesticides (Kang et al., 2014). Systemic exposure cannot explain their apparent MN specificity, although exposure through skin abrasions to hands of feet could in principal promote reverse axonal transport (Bisby and Bulger, 1977) and their delivery directly into spinal cord MN (Wiley et al., 1982). This model also suggests strategies for prevention such as including axon transport inhibitors in agrochemical stocks or using retrograde transport to deliver candidate MN therapeutics such as neurotrophins (Kaspar et al., 2003). The injury model outlined in this study provides a strategy to initiate such studies.

Acknowledgments: *We thank Fang Li and Dong Jiang (Soochow University, Suzhou PRC) for pilot studies on sciatic nerve suicide transport, Huaye Zhang and Vicky DiBona for Thy1-eGFP transgenic mice, and Raco Rasin for stocks of PRV-eGFP and PRV-mRFP.*
Author contributions: *CAC and RDM performed all surgical procedures, ASL contributed to histology, JEP performed the motor function, and RDM wrote the manuscript.*
Conflicts of interest: *The authors declare no conflict of interests.*
Financial support: *Supported by grants to Dr McKinnon (PI) from the New Jersey Commission on Spinal Cord Research (05-3047; 11-015).*
Institutional review board statement: *All procedures were performed at Rutgers under established Institutional Animal Care and Use protocols (eIACUC_TR201800022, approved on March 20, 2018).*
Copyright license agreement: *The Copyright License Agreement has been signed by all authors before publication.*
Data sharing statement: *Datasets analyzed during the current study are available from the corresponding author on reasonable request.*
Plagiarism check: *Checked twice by iThenticate.*
Peer review: *Externally peer reviewed.*

References

Arriola A, Kiel ME, Shi YF, McKinnon RD (2010) Adjunctive MSCs enhance myelin formation by xenogenic oligodendrocyte precursors transplanted in the retina. Cell Res 20:728-731.
Bao F, Liu D (2002) Peroxynitrite generated in the rat spinal cord induces neuron death and neurological deficits. Neuroscience 115:839-849.
Basso DM, Beattie MS, Bresnahan JC (1995) A sensitive and reliable locomotor rating scale for open field testing in rats. J Neurotrauma 12:1-21.
Bisby MA, Bulger VT (1977) Reversal of axonal transport at a nerve crush. J Neurochem 29:313-320.
Bruijn LI, Miller TM, Cleveland DW (2004) Unraveling the mechanisms involved in motor neuron degeneration in ALS. Annu Rev Neurosci 27:723-749
Card JP, Enquist LW (2012) Use and visualization of neuroanatomical viral transneuronal tracers. In: Visualization techniques. Neuromethods, vol 70 (Badoer E, ed). Humana Press, Totowa, NJ.
Cheriyan T, Ryan DJ, Weinreb JH, Cheriyan J, Paul JC, Lafage V, Kirsch T, Errico TJ (2014) Spinal cord injury models: a review. Spinal Cord 52:588-595.
Dietz V, Schwab ME (2017) From the Rodent Spinal Cord Injury Model to Human Application: Promises and Challenges. J Neurotrauma 34:1826-1830.
Ebner S, Dunbar M, McKinnon RD (2000) Distinct roles for PI3K in proliferation and survival of oligodendrocyte progenitor cells. J Neurosci Res 62:336-345.
Harper CG, Gonatas JO, Mizutani T, Gonatas NK (1980) Retrograde transport and effects of toxic ricin in the autonomic nervous system. Lab Invest 42:396-404.
Harrison M, O'Brien A, Adams L, Cowin G, Ruitenberg MJ, Sengul G, Watson C (2013) Vertebral landmarks for the identification of spinal cord segments in the mouse. Neuroimage 68:22-29.
Hillyer JE, Joynes RL (2009) A new measure of hindlimb stepping ability in neonatally spinalized rats. Behav Brain Res 202:291-302.
Kang H, Cha ES, Choi GJ, Lee WJ (2014) Amyotrophic lateral sclerosis and agricultural environments: a systematic review. J Korean Med Sci 29:1610-1617.
Kaspar BK, Llado J, Sherkat N, Rothstein JD, Gage FH (2003) Retrograde viral delivery of IGF-1 prolongs survival in a mouse ALS model. Science 301:839-842.
Kiel ME, Chen CP, Sadowski D, McKinnon RD (2008) Stem cell-derived therapeutic myelin repair requires 7% cell replacement. Stem Cells 26:2229-2236.
Kjell J, Olson L (2016) Rat models of spinal cord injury: from pathology to potential therapies. Dis Model Mech 9:1125-1137.
Lemmon VP, Abeyruwan S, Visser U, Bixby JL (2014) Facilitating transparency in spinal cord injury studies using data standards and ontologies. Neural Regen Res 9:6-7.
Liang Y, Zhang J, Walczak P, Bulte JWM (2018) Quantification of motor neuron loss and muscular atrophy in ricin-induced focal nerve injury. J Neurosci Methods 308:142-150.
Liu D, Xu GY, Pan E, McAdoo DJ (1999) Neurotoxicity of glutamate at the concentration released upon spinal cord injury. Neuroscience 93:1383-1389.
Liu NK, Zhang YP, Titsworth WL, Jiang X, Han S, Lu PH, Shields CB, Xu XM (2006) A novel role of phospholipase A2 in mediating spinal cord secondary injury. Ann Neurol 59:606-619.
Livak KJ, Schmittgen TD (2001) Analysis of relative gene expression data using real-time quantitative PCR and the 2(T)(-Delta Delta C) method. Methods 25:402-408.
Minakov AN, Chernov AS, Asutin DS, Konovalov NA, Telegin GB (2018) Experimental models of spinal cord injury in laboratory rats. Acta Naturae 10:4-10.
Okabe N, Himi N, Maruyama-Nakamura E, Hayashi N, Narita K, Miyamoto O (2017) Rehabilitative skilled forelimb training enhances axonal remodeling in the corticospinal pathway but not the brainstem-spinal pathways after photothrombotic stroke in the primary motor cortex. PLoS One 12:e0187413.
Savastano LE, Laurito SR, Fitt MR, Rasmussen JA, Gonzalez Polo V, Patterson SI (2014) Sciatic nerve injury: a simple and subtle model for investigating many aspects of nervous system damage and recovery. J Neurosci Methods 227:166-180.
Snow DM (2014) Commentary on: "Facilitating transparency in spinal cord injury studies using data standards and ontologies". Neural Regen Res 9:8-9.
Walker EH, Pacold ME, Perisic O, Stephens L, Hawkins PT, Wymann MP, Williams RL (2000) Structural determinants of phosphoinositide 3-kinase inhibition by wortmannin, LY294002, quercetin, myricetin, and staurosporine. Mol Cell 6:909-919.
Watson BD, Prado R, Dietrich WD, Ginsberg MD, Green BA (1986) Photochemically induced spinal cord injury in the rat. Brain Res 367:296-300.
Wiley RG, Blessing WW, Reis DJ (1982) Suicide transport: destruction of neurons by retrograde transport of ricin, abrin, and modeccin. Science 216:889-890.
Wiley RG, Oeltmann TN (1986) Anatomically selective peripheral nerve ablation using intraneural ricin injection. J Neurosci Methods 17:43-53.
Yamamoto T, Iwasaki Y, Konno H, Kudo H (1985) Primary degeneration of motor neurons by toxic lectins conveyed from the peripheral nerve. J Neurol Sci 70:327-337.

C-Editors: Zhao M, Li CH; T-Editor: Jia Y